Research Article | Vol. 25, No. 17 | 21 Aug 2017 | OPTICS EXPRESS 20556
Optics EXPRESS

Analysis of spurious diffraction orders of computer-generated hologram in symmetric aspheric metrology

YIWEI HE,[1,2,3,*] XI HOU,[1] FAN WU,[1] XINXUE MA,[4] AND RONGGUANG LIANG[2]

[1]*The Institute of Optics and Electronics, Chinese Academy of Sciences, Chengdu, Sichuan 610209, China*
[2]*College of Optical Sciences, University of Arizona, Tucson, AZ 85721, USA*
[3]*University of Chinese Academy of Sciences, Beijing 100039, China*
[4]*Changchun Institute of Optics, Fine Mechanics and Physics, Chinese Academy of Sciences, Changchun 130033, China*
**heyiwei1224@163.com*

Abstract: Computer-generated hologram (CGH) has been widely used as a wavefront compensator in symmetric aspheric metrology. As a diffractive element, it generates different diffraction orders, but only the 1st-order diffraction is used to test aspheric surface. The light from spurious diffraction orders (SDO) will produce many high-frequency fringes in interferogram and reduce measurement accuracy. In this paper, we regard the CGH null system as an imaging system and develop an aberration model in Seidel formalism to analyze the SDO. This model has the advantage to address the difference between the SDO (k_1, k_2) and (k_2, k_1). We consider the effect of the pupil distortion so that our model can analyze the SDO with a large pupil distortion. We derive the condition to ensure the 2nd-order and 4th-order aberrations have the same sign and calculate the minimum defocused distance (power carrier frequency) of CGH. According to the marginal-ray heights (h_1 and h_3) on the CGH in the first and second passes, we determine the condition that the SDO covers the whole CGH in the second pass. We analyze the SDO of 4 CGH designs and compare the results from our aberration model with these from real ray trace. These results validate that our aberration model is feasible whether the aspheric part is convex or concave and whether CGH is inside or outside the focus of the transmission sphere.

OCIS codes: (220.1250) Aspherics; (120.6650) Surface measurements, figure; (120.2880) Holographic interferometry.

References and links

1. A. J. MacGovern and J. C. Wyant, "Computer generated holograms for testing optical elements," Appl. Opt. **10**(3), 619–624 (1971).
2. P. Zhou and J. H. Burge, "Optimal design of computer-generated holograms to minimize sensitivity to fabrication errors," Opt. Express **15**(23), 15410–15417 (2007).
3. S. Li, B. Liu, A. Tian, Z. Guo, P. Yang, and J. Zhang, "A practical method for determining the accuracy of computer-generated holograms for off-axis aspheric surfaces," Opt. Lasers Eng. **77**, 154–161 (2015).
4. Z. Gao, M. Kong, R. Zhu, and L. Chen, "Problems on design of computer-generated holograms for testing aspheric surfaces: principle and calculation," Chin. Opt. Lett. **5**(4), 241–244 (2007).
5. S. Peterhänsel, C. Pruss, and W. Osten, "Phase errors in high line density CGH used for aspheric testing: beyond scalar approximation," Opt. Express **21**(10), 11638–11651 (2013).
6. N. Lindlein, "Analysis of the disturbing diffraction orders of computer-generated holograms used for testing optical aspherics," Appl. Opt. **40**(16), 2698–2708 (2001).
7. P. Zhou, W. Cai, C. Zhao, and J. H. Burge, "Parameteric definition for the CGH patterns and error analysis in interferometric measurements," Proc. SPIE **8415**, 841505 (2012).
8. J. Peng, J. Ren, X. Zhang, and Z. Chen, "Analytical investigation of the parasitic diffraction orders of tilt carrier frequency computer-generated holograms," Appl. Opt. **54**(13), 4033–4041 (2015).
9. M. Born and E. Wolf, *Principles of Optics* (Publishing House of Electronics Industry, 2009), Ch. 4–5.

#296198 https://doi.org/10.1364/OE.25.020556
Journal © 2017 Received 17 May 2017; revised 23 Jul 2017; accepted 27 Jul 2017; published 15 Aug 2017

Optics EXPRESS

1. Introduction

Compared with spherical surface, aspheric surface can improve the performance of the optical system and reduce its complexity, so it is widely used in modern optical systems, such as astronomical telescopes and photolithographic lenses. However, since aspheric surface is not self-collimated under spherical wavefront, i.e., the testing rays do not impinge normally on aspheric part, it cannot be directly tested under standard interferometer. Computer-generated hologram (CGH) is often inserted between the aspheric part and the transmission sphere to transfer spherical wavefront to match the aspheric one [1–3].

As a diffractive element, CGH generates many diffraction orders, but only the first diffraction order is used to test aspheric part. The rays from the spurious diffraction orders (stray rays) will produce many high-frequency fringes in interferogram and reduce measurement accuracy [4]. Since the stray rays pass through CGH twice, we denote the spurious diffraction orders (SDO) as (k_1, k_2), where k_1 and k_2 is the diffraction order of CGH in the first and second pass, respectively. To decrease the effect of SDO, power and tilt carrier frequency are usually added to CGH, so SDO can be separated large enough and then be blocked by the inner pinhole filter. However, excessive carrier frequency also results in small line space on CGH and drives up the cost [5].

The SDO has been investigated in past 20 years. In 2001, N. Lindlein derived the 1st-order ray model to analyze the SDO of symmetric CGH when testing convex aspheric part and CGH was laid close to convex aspheric part [6]. They argued the SDO (−1, 3) and (3, −1) has the most significant effect on measurement accuracy and calculated the minimum amount of power carrier frequency to separate SDO. In 2012, P. Zhou et al [7] developed the parameter model to describe the CGH null system in power carrier frequency and calculated the distance from the pinhole to its paraxial image. This distance was used to evaluate the separation of SDO. In 2015, J. Peng et al. [8] introduced a tilt quantity into Zhou's parameter model, so it can be used to describe the CGH null system with tilt carrier frequency. On the other side, they included a scale factor between CGH size and aspheric part in Lindlein's model, so Lindlein's model can analyze SDO whether CGH is close to aspheric part or not. Using these two models, they analyzed the SDO of non-symmetric CGH and calculated the minimum amount of tilt carrier frequency when testing conic surfaces with a large F# (larger than 4). They proposed the necessary condition to separate SDO by tilt carrier frequency when testing paraboloid: the paraxial center of the paraboloid should be inside the focus of transmission sphere. They observed that the SDO (2, 0) has a better agreement of ray error on pinhole with the real ray error than the SDO (0, 2). They also observed one of the SDO (k_1, k_2) and (k_2, k_1) cannot cover the CGH in the second pass.

Lindlein's model has made a great advance in the analysis of SDO. However, because of the 1st-order approximation, this model shows no difference between the SDO (k_1, k_2) and (k_2, k_1). Usually only one of the SDO (k_1, k_2) and (k_2, k_1) agrees well with the real ray trace. The function between the CGH coordinate and the ray error on pinhole in this model is single-valued while in reality, because of the negative distortion, this function could be multi-valued, i.e., it is possible that two rays pass the CGH at the same point. Therefore, we develop a new aberration model in Seidel formalism to analyze the SDO. This model has the advantage to address the difference between the SDO (k_1, k_2) and (k_2, k_1). Since our model considers the effect of the pupil distortion, even if there are two rays passing the same point on the CGH in the second pass, the ray error calculated by our model also agrees well with that calculated by real ray trace. In our model, we derive the condition to ensure the 2^{nd}-order and 4^{th}-order aberrations have the same sign, so we can avoid the risk that the outer annular of CGH is disturbed by spurious diffraction orders. We also calculate the minimum defocused distance (power carrier frequency) of CGH. According to the marginal-ray heights on the CGH in the first and second pass, we provide an equation to determine what kinds of SDO can cover the whole CGH in the second pass.

Optics EXPRESS

In this paper, we first introduce three basic layouts of CGH when testing concave and convex aspheric part. Then we derive the principles of our aberration model in Section 3. The aberration model is furtherly simplified in Section 4 so the qualitative analysis can be conducted. The qualitative analysis provides the guidance for CGH design. According to the three basic layouts of CGH in Section 2, we design four different CGHs and analyze their SDO in Section 5. The ray error on pinhole calculated by our model is compared with that calculated by real ray trace to validate our model.

2. Three basic layouts of CGH to test concave or convex aspheric part

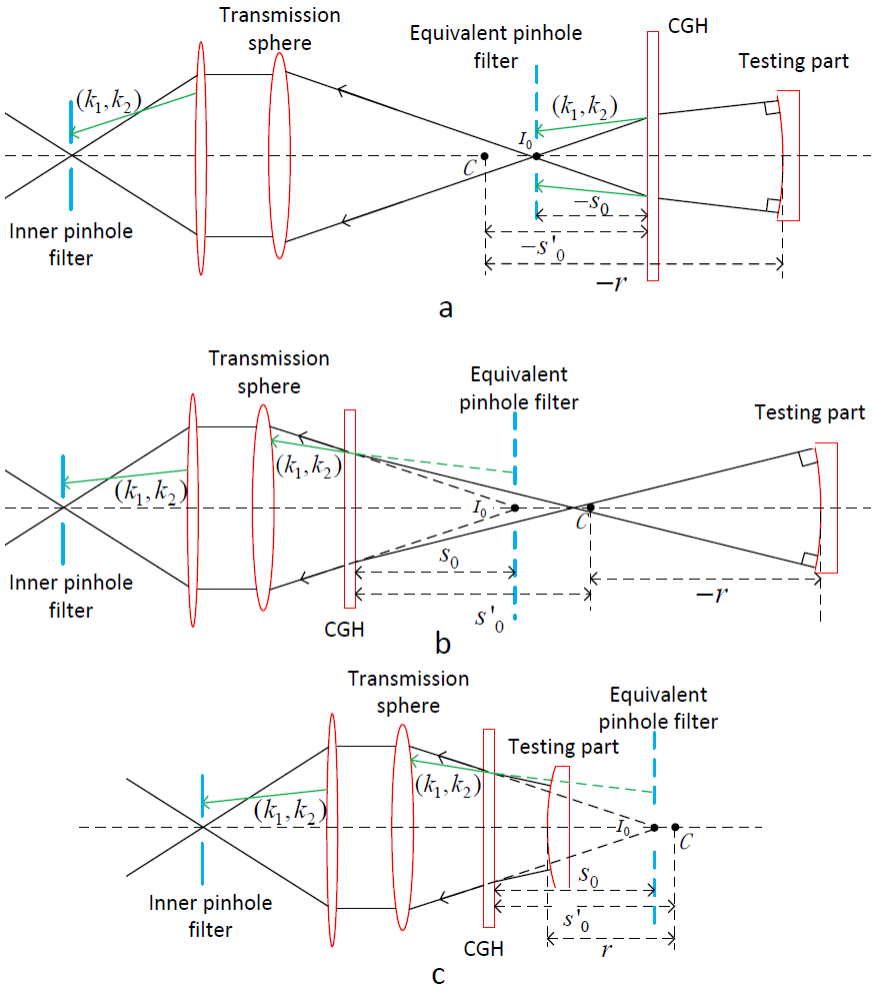

Fig. 1. Three basic layouts of CGH.

There are three basic layouts of CGH to test concave or convex aspheric part, shown in Fig. 1. The layouts in Figs. 1(a) and 1(b) are used to test concave part while the layout in Fig. 1(c) is used to test convex one. CGHs in Figs. 1(a) and 1(b) are outside and inside the focus I_0 of the transmission sphere, respectively. The equivalent pinhole filter is an image of the inner pinhole filter. k_1, k_2 are the diffraction orders in the first and second pass through CGH, respectively. s_0 is the distance from CGH to the focus I_0, s'_0 is the distance from CGH to the paraxial center C of the testing part and r is the base-sphere radius of the testing part. The negative sign means the point C or I_0 is at the left side of CGH. Since $d = s'_0 - r$ (d is the

Optics EXPRESS

distance from CGH to the testing part), for a specified aspheric part (r is given), the layout of CGH is determined by the variables s_0 and s'_0. It is easy to have $r < s_0 < 0$ and $r < s'_0 < 0$ in Fig. 1(a), $s_0 > 0$, $s'_0 > 0$ and $r < 0$ in Fig. 1(b), and $0 < r < s_0$ and $0 < r < s'_0$ in Fig. 1(c). In Section 5, we will show how the quantities s_0, s'_0 and r affect the CGH design and its SDO in these three layouts.

3. The aberration model in Seidel formalism

The interferometer images the CGH to its CCD plane, so the disturbed area on CGH is also the disturbed area of testing data on CCD. On the other side, CGH null system can be treated as three imaging subsystems shown in Fig. 2. The focus I_0 of the transmission sphere is first imaged to I_1 by CGH (the first subsystem), then I_1 is imaged to I_2 by the testing part (the second subsystem), and I_2 is finally imaged to I_3 by the CGH again (the third subsystem). For convenience in discussing the disturbed area on CGH, we assume the exit pupil of the CGH null system is placed on CGH in the image space of the third subsystem. Its semi-diameter in the objective and image space of the i^{th} subsystem is λ_i and λ'_i, respectively. The focal lengths of the first and third subsystems are determined by the diffraction order and the added optical path of CGH phase function. For the diffraction orders (+ 1, + 1), I_3 is the perfect image of I_0 and coincides with I_0, which can be used to gain the added optical path of CGH phase function in the following discussion.

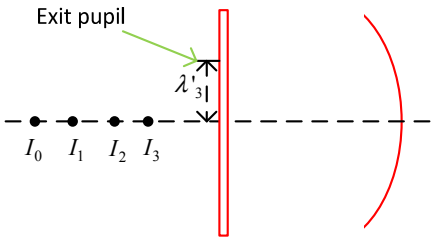

Fig. 2. The imaging schematic of the CGH null system.

3.1 The Seidel variable and its relationship with the ray vector

A general imaging system is shown in Fig. 3. The object plane, image plane, entrance pupil, and exit pupil are located at the on-axis point *A, B, D,* and *E*, respectively. The ray intersects with the object plane, image plane, entrance pupil and exit pupil at A'', B'', D'', E'', respectively. The perpendicular foot from *A, B* to the ray is A', B', respectively. The heights of the object plane and its image plane are τ and τ', respectively; the heights of the entrance pupil and exit pupil are λ and λ', respectively; the distance from the principal plane to the object plane is s and its conjugated distance is s'; the distance from the principal plane to the entrance pupil is t and its conjugated distance is t'; the distance from the object plane to the entrance pupil is g and its conjugated distance is g'. The Seidel variables of the paraxial ray are defined as

$$\left.\begin{aligned} \chi = \psi\frac{x_o}{\tau}, \chi' = \psi\frac{x'_o}{\tau'} \\ \xi = \frac{x_e}{\lambda}, \xi' = \frac{x'_e}{\lambda'} \end{aligned}\right\} \quad (1)$$

Optics EXPRESS

where x_o, x'_o, x_e and x'_e are the X-axis coordinates of paraxial ray on the object plane, image plane, entrance pupil and exit pupil, respectively (for the ray in Fig. 3, x_o, x'_o, x_e and x'_e are the X-axis coordinates of A'', B'', D'', E'', respectively); the Lagrange-Helmholtz invariable ψ is $\psi = \frac{n\tau\lambda}{g} = \frac{n'\tau'\lambda'}{g'}$ [9]. From the definition, the Seidel variable ξ is the normalized pupil coordinate and the Seidel variable $\chi = n\lambda\frac{x_o}{g}$ is the intersection angle $\angle A''DA$, multiplied by the refractive index and entrance pupil height. The advantage of using the Seidel variables, not the regular pupil coordinates, is that the aberration coefficient of the total system is the sum of the aberration coefficients of its subsystems only when using the Seidel variables [9].

The ray vector is defined as $(p,m)=(n\cos\alpha, n\cos\gamma)$, where n is the refractive index and (α,γ) is the direction angle of the ray along X and Z axis, shown in Fig. 3. The ray vector can be expressed by the Seidel variables

$$\left.\begin{aligned} p &= n\left(\frac{h}{s}\xi - \frac{H}{t}\chi\right), m = n\sqrt{1-\left(\frac{p}{n}\right)^2} \\ p' &= n'\left(\frac{h'}{s'}\xi' - \frac{H'}{t'}\chi'\right), m' = n'\sqrt{1-\left(\frac{p'}{n'}\right)^2} \end{aligned}\right\} \tag{2}$$

where $h = \frac{\lambda s}{g}, h' = \frac{\lambda' s'}{g'}, H = \frac{t}{\lambda n}, H' = \frac{t'}{\lambda' n'}$; n and n' are the refractive indices in the object and image spaces, respectively. It is easy to see h and h' are the heights of the principal plane in the object and image space, respectively. For the thin imaging element, the principal plane coincides with the imaging element, so h is also the paraxial height of the marginal ray on the imaging element (the marginal ray is the ray passing the edge of exit pupil and the center of the field). In Gaussian optics, we have $\chi = \chi', \xi = \xi', h = h', H = H'$.

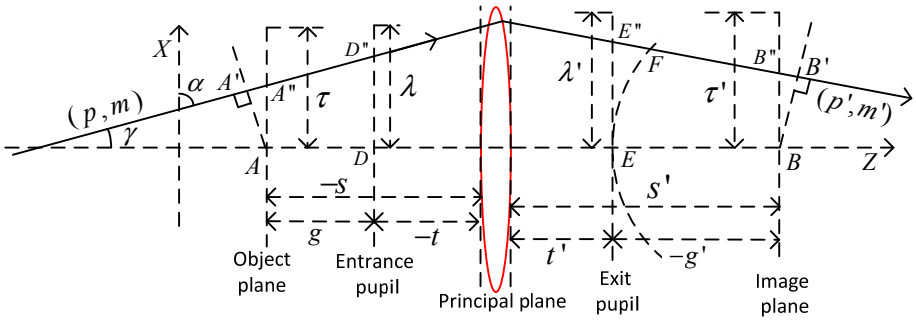

Fig. 3. A general imaging system.

3.2 Relationship between the 4th-order angular characteristic function and the 4th-order aberration

For a general imaging system in Fig. 3, B is the Gaussian image point of A. The sphere EF is centered at B point and called the Gaussian reference sphere. The angular characteristic function (ACF) of ray $A'B'$ is defined as the optical path difference (OPD) between ray $A'B'$ and chief ray AB, i.e., $T_{A'B'} = op(A',B') - op(A,B)$, where $T_{A'B'}$ is the ACF of ray

$A'B'$ and $op(A,B)$ is the optical path between A and B. Assuming there is a ray linking A and F, the aberration W_F at F point is defined as the OPD between ray AF and chief ray AE, i.e., $W_F = op(A,F) - op(A,E)$. When A' coincides with A, we have

$$T_{A'B'} = W_F + l_{FB'} - l_{EB} \tag{3}$$

where l_{EB} is the distance between E point and B point. Since B is the Gaussian image point of A, $l_{FB'} - l_{EB}$ is a quantity with its order higher than 4, which means

$$T^{(4)}_{A'B'} = W^{(4)}_F, \tag{4}$$

where $T^{(4)}$ and $W^{(4)}$ are referred to as the 4th-order parts of T and W.

3.3 The angular characteristic functions of three subsystems

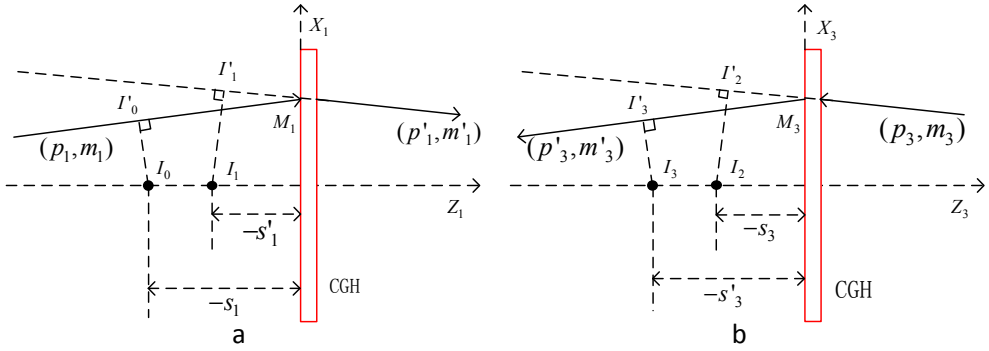

Fig. 4. The schematic to calculate ACF of two subsystems. (a): the first subsystem; (b): the third subsystem.

How to calculate the ACF of the first subsystem is shown in Fig. 4(a). The ray $I'_0 I'_1$ intersects with CGH at M_1 and the point I'_0 and I'_1 is the perpendicular foot from I_0 and I_1 to the ray, respectively. The coordinates of I_0, I_1 and M_1 are $(0,s_1)$, $(0,s'_1)$ and $(x_1,0)$, respectively and s_1 is always equal to s_0. It is easy to have

$$\begin{aligned} T_{I_0'I_1'} &= \overrightarrow{I_0M_1}\cdot(p_1,m_1) + \overrightarrow{M_1I_1}\cdot(p'_1,m'_1) + k_1\varphi(x_1) \\ &= x_1p_1 + (-s_1)m_1 + (-x_1)p'_1 + s'_1\,m'_1 + k_1\varphi(x_1) \end{aligned} \tag{5}$$

where $T_{I_0'I_1'}$ is the ACF of the ray $I_0'I_1'$, $\varphi(x_1)$ is the added optical path of CGH phase function and the symbol $\cdot$ is the scalar product. In the 4th-order approximation, we have

$$\left.\begin{aligned} \varphi(x_1) &= -\frac{x_1^2}{2a} - \frac{x_1^4}{8b^3} \\ m_1 &= n_1\sqrt{1-\left(\frac{p_1}{n_1}\right)^2} = 1 - \frac{p_1^2}{2} - \frac{p_1^4}{8} \\ m'_1 &= n'_1\sqrt{1-\left(\frac{p'_1}{n'_1}\right)^2} = 1 - \frac{p'^2_1}{2} - \frac{p'^4_1}{8} \end{aligned}\right\}, \tag{6}$$

Optics EXPRESS

where the refractive indices $n_1 = n'_1 = 1$ in this subsystem. According to eikonal equation, we have

$$k_1 \frac{\partial \varphi_1}{\partial x_1} = p'_1 - p_1 = k_1(-\frac{x_1}{a} - \frac{x_1^3}{2b^3}). \tag{7}$$

Solving Eq. (7) in the 4th-order approximation, we have

$$x_1 = -\frac{a}{k_1}(p'_1 - p_1) + \frac{a^4}{2k_1^3 b^3}(p'_1 - p_1)^3. \tag{8}$$

Substituting Eq. (6), 8) into Eq. (5), the ACF of the first subsystem in the 4th-order approximation is

$$T^{(4)}_{I_0'I_1'} = -\frac{a^4}{8b^3 k_1^3}(p'_1 - p_1)^4 - \frac{1}{8}(s'_1 p'^4_1 - s_1 p_1^4). \tag{9}$$

With a similar procedure, the 4th-order ACF of the third subsystem in Fig. 4(b) is

$$T^{(4)}_{I_2'I_3'} = -\frac{a^4}{8b^3 k_2^3}(p'_3 - p_3)^4 + \frac{1}{8}(s'_3 p'^4_3 - s_3 p_3^4), \tag{10}$$

where the positive sign is because of $m_3 < 0$ and $m'_3 < 0$.

The aspheric surface in the second subsystem is regarded as a deformed mirror, shown in Fig. 5. In the 4th-order approximation the aspheric surface can be expressed as

$$z_2 = \frac{x_2^2}{2r} + \frac{x_2^4}{8r^3}(1 + b_m), \tag{11}$$

where b_m is the deformed factor of the aspheric surface.

The ACF of a deformed mirror has been discussed in [9] as

$$T^{(4)}_{I'_1 I'_2} = \frac{(1+b_m)r}{64}(p'_2 - p_2)^4 + \frac{s'_2 p'^4_2 + s_2 p_2^4}{8} - \frac{r}{16}(p'_2 - p_2)^2(p'^2_2 + p_2^2). \tag{12}$$

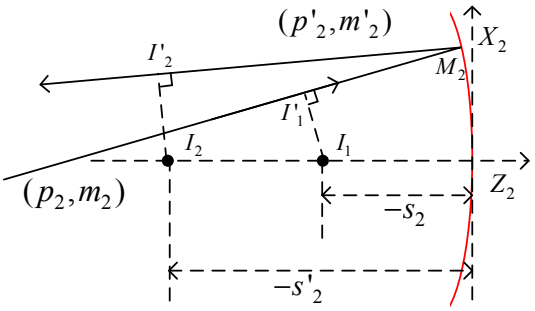

Fig. 5. The schematic of the second subsystem to calculate ACF

3.4 The total 4th-order aberration coefficient

The 4th-order aberration is equal to the 4th-order ACF shown in Eq. (4). Since the aberration is expressed with the exit pupil variable, not the ray direction, to obtain the aberration coefficients, these ray-direction variables in Eqs. (9), (10), and (12) should be replaced by the exit pupil variables. Besides, the imaging equation is

Optics EXPRESS

$$\left.\begin{array}{l}\frac{1}{s'_1}-\frac{1}{s_1}=\frac{k_1}{a},\frac{1}{s'_2}+\frac{1}{s_2}=\frac{2}{r},\frac{1}{s_3}-\frac{1}{s'_3}=\frac{k_2}{a}\\ \frac{1}{t'_1}-\frac{1}{t_1}=\frac{k_1}{a},\frac{1}{t'_2}+\frac{1}{t_2}=\frac{2}{r},\frac{1}{t_3}-\frac{1}{t'_3}=\frac{k_2}{a}\end{array}\right\}, \tag{13}$$

where s_i, s'_i, t_i, t'_i have the same definition as s, s', t, t' in Section 3.1 and the subscript i indicates the quantities belong to the i^{th} subsystem.

Substituting Eqs. (2) and (13) into Eqs. (9), (10) and (12) and only considering the ξ^4 term, the total 4th-order aberration is

$$\begin{aligned}W^{(4)} &= w_{040}\xi^4 = T^{(4)}_{I_0'I_3'} = T^{(4)}_{I_0'I_1'} + T^{(4)}_{I_1'I_2'} + T^{(4)}_{I_2'I_3'}\\ &= -\frac{k_1}{8b^3}h_1^4\xi^4 - \frac{1}{8}\left(\frac{1}{s'^3_1}-\frac{1}{s_1^3}\right)h_1^4\xi^4\\ &\quad -\frac{k_2}{8b^3}h_3^4\xi^4 + \frac{1}{8}\left(\frac{1}{s'^3_3}-\frac{1}{s_3^3}\right)h_3^4\xi^4\\ &\quad +\frac{1}{4}\left[\frac{b_m}{r^3}+\frac{1}{r}\left(\frac{1}{r}-\frac{1}{s_2}\right)^2\right]h_2^4\xi^4\end{aligned} \tag{14}$$

where h_i has the same definition as h in Section 3.1 and the subscript i indicates the quantity belongs to the i^{th} subsystem. Using the definition of h, we have $\frac{h_{i+1}}{h_i}=\frac{s_{i+1}}{s'_i}$.

When the diffraction orders are (+ 1, + 1), I_3 point is the perfect image of I_0 point and coincides with I_0, which means

$$s_1 = s_0, s'_1 = s'_0, s_2 = s'_2 = r, s_3 = s'_0, s'_3 = s_0. \tag{15}$$

Substituting Eq. (15) into Eq. (14) and using $w_{040}=0$ and $\frac{h_{i+1}}{h_i}=\frac{s_{i+1}}{s'_i}$, we obtain the 4th-order coefficient of the added optical path $\varphi(x)$ of CGH phase function

$$\frac{1}{b^3}=\frac{1}{s_0^3}-\frac{1}{s'^3_0}+b_m\frac{r}{s'^4_0}. \tag{16}$$

3.5 The change of the reference sphere

As shown in Fig. 6, the sphere sp_1, centered at the Gaussian image point I_3, is the Gaussian reference sphere and the sphere sp_2, centered at the focus I_0 (cat eye), is the cat-eye reference sphere. The ray intersects with sp_1 and sp_2 at N_1 and N_2, respectively. The aberration in Eq. (14) is observed at the sphere sp_1, but to analyze the spurious diffraction orders, we need to obtain the aberration coefficients at the sphere sp_2. This change of the reference sphere results in an extra aberration $l_{N_1N_2}$ that mainly consists of the 2nd-order aberration:

$$l_{N_1N_2} \approx W^{(2)} = w_{020}\xi^2 = \frac{h_3^2}{2}\left(\frac{1}{s'_3}-\frac{1}{s_0}\right)\xi^2. \tag{17}$$

Optics EXPRESS

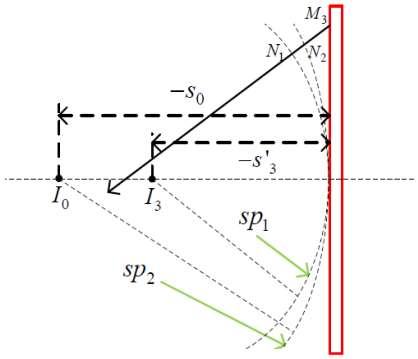

Fig. 6. The change of the reference sphere

3.6 The total aberration up to four orders and its ray error

By summing Eqs. (14) and (17), we have the total wavefront aberration of CGH null system:

$$W = w_{020}\xi^2 + w_{040}\xi^4. \tag{18}$$

The ray error e_{ray} of the spurious diffraction orders is calculated from the differentiation of the wave-front aberration:

$$e_{ray} = -s_0 \frac{\partial W}{\lambda'_3 \partial \xi}. \tag{19}$$

When the ray error is larger than the semi-diameter of the equivalent pinhole filter, the stray ray cannot disturb the testing results.

3.7 The pupil distortion

We assume the height of ray on the exit pupil is x_3 in paraxial ray trace and $\overline{x_3}$ in real ray trace. According the Seidel theory, we have

$$\overline{\xi} - \xi = \frac{\partial T^{(4)}_{I_0'I_3'}}{\partial \chi} \tag{20}$$

where $\overline{\xi}$ and ξ are the Seidel variables of real ray and paraxial ray and $\overline{\xi} = \frac{\overline{x_3}}{\lambda_3}, \xi = \frac{x_3}{\lambda_3}$.

Therefore the pupil distortion is

$$\overline{x_3} - x_3 = \lambda_3 \frac{\partial T^{(4)}_{I_0'I_3'}}{\partial \chi}. \tag{21}$$

Substituting Eqs. (2) and (13) into Eqs. (9), (10), and (12), and only considering the $\chi\xi^3$ term, the pupil distortion in Eq. (21) is expressed as

$$\begin{aligned}\overline{x_3} - x_3 = {} & \frac{1}{2}\left(\frac{k_1}{b^3} + \frac{1}{s'^2_1 t'_1} - \frac{1}{s_1^2 t_1}\right) h_1^3 \xi^3 H_1 \lambda_3 + \frac{1}{2}\left(\frac{k_2}{b^3} - \frac{1}{s'^2_3 t'_3} + \frac{1}{s_3^2 t_3}\right) h_3^3 \xi^3 H_3 \lambda_3 \\ & - \left[\frac{b_m}{r^3} + \frac{1}{r}\left(\frac{1}{r} - \frac{1}{s_2}\right)\left(\frac{1}{r} - \frac{1}{t_2}\right)\right] h_2^3 \xi^3 H_2 \lambda_3\end{aligned} \tag{22}$$

Optics EXPRESS

where H_i has the same definition as H in Section 3.1 and the subscript i indicates the quantities belong to the i^{th} subsystem.

4. The qualitative discussion of spurious diffraction order

4.1 The expansion of the aberration coefficients

To discuss what kinds of spurious diffraction orders have the most significant disturbing on testing data, we expand these coefficients in Eqs. (14) and (17) into a series of $\sum_i \frac{c_i}{a^i}$ in the following procedure.

Firstly, we calculate the deviation of the Gaussian image point of SDO from the testing-ray image point. Using Eq. (13), it is easy to obtain

$$\Delta s'_1 = \Delta s_2 = s'_1 - s'_0 = \frac{s_1}{1+\frac{k_1}{a}s_1} - \frac{s_1}{1+\frac{1}{a}s_1} = (1-k_1)\frac{s_1^2}{a} - (1-k_1^2)\frac{s_1^3}{a^2} + o(\frac{1}{a^3}) \quad (23)$$

where $o(\frac{1}{a^3})$ is a small quantity having the same order with $\frac{1}{a^3}$. Similarly, we have

$$\left.\begin{aligned} \Delta s'_2 = \Delta s_3 = s'_2 - r = (k_1-1)\frac{s_1^2}{a} - (k_1^2-1)\frac{s_1^3}{a^2} + (k_1-1)^2\frac{2s_1^4}{ra^2} + o(\frac{1}{a^3}) \\ \Delta s'_3 = s'_3 - s_0 = (k_1+k_2-2)\frac{s_1^2}{a} + (k_1-1)^2\frac{2s_1^4}{ra^2} + [2(k_2-1)^2 - (k_1-k_2)^2]\frac{s_1^3}{a^2} + o(\frac{1}{a^3}) \end{aligned}\right\}. \quad (24)$$

Substituting Eqs. (23) and (24) into Eqs. (14) and (17) and using $s_1 = s_0$, the 2[nd]-order and 4[th]-order aberration coefficients can be expressed as

$$\left.\begin{aligned} \frac{w_{020}}{h_3^2} &= \frac{2-k_1-k_2}{2a} + o(\frac{1}{a^2}), \text{ at } k_1 - k_2 \neq 2 \\ \frac{w_{020}}{h_3^2} &= (1-k_1)^2(1-\frac{s_0}{r})\frac{s_0}{a^2} + o(\frac{1}{a^3}), \text{ at } k_1 - k_2 = 2 \\ \frac{w_{040}}{h_3^4} &= \frac{(2-k_1-k_2)}{8} b_m \frac{r}{s'^4_0} + o(\frac{1}{a}), \text{ at } k_1 - k_2 \neq 2 \\ \frac{w_{040}}{h_3^4} &= -(1-k_1)^2(1-\frac{r}{s'_0}) b_m \frac{s_0^2}{a s'^4_0} + o(\frac{1}{a^2}), \text{ at } k_1 - k_2 = 2 \end{aligned}\right\}. \quad (25)$$

Using $\frac{h_{i+1}}{h_i} = \frac{s_{i+1}}{s'_i}$, we derive

$$\frac{h_1}{h_3} = \frac{s'_1 s'_2}{s_3 s_2} \approx 1 + (\frac{1}{r} - \frac{1}{s'_0})(\Delta s'_2 - \Delta s'_1) \approx 1 + 2(\frac{1}{r} - \frac{1}{s'_0})(s_0 - s'_0)(k_1 - 1). \quad (26)$$

According to the discussion in Section 3.1, h_1 and h_3 are the marginal-ray heights on the CGH in the first and second passes, respectively, so the ratio $\left|\frac{h_1}{h_3}\right|$ determines whether the CGH in the second pass is completely covered.

Optics EXPRESS

4.2 The qualitative discussion of SDO in three different CGH layouts

We carry out the qualitative discussion from the following four aspects: the ray error on equivalent pinhole filter, the sign of aberration coefficients, the ratio $\left|\frac{h_1}{h_3}\right|$ and the minimum amount of power carrier frequency.

Firstly, the ray error on equivalent pinhole filter. For the SDO $(k_1 \neq 1, k_2 \neq 1)$, if the ray error is smaller than the semi-diameter of the pinhole filter, the ray could not be blocked and would disturb the corresponding testing area. Because of $\frac{1}{a^2}$ $\frac{1}{a^1}$ $\frac{1}{a^0}$, from Eq. (25) we find the SDO with $k_1 + k_2 = 2$ has the smaller aberration coefficients and ray error than those with $k_1 + k_2 \neq 2$, i.e., the SDO with $k_1 + k_2 = 2$ is more difficult to separate than these SDO with $k_1 + k_2 \neq 2$. Besides, in practice, the CGH is usually the Ronchi phase grate with the duty cycle $\frac{1}{2}$, which makes the even diffraction orders have zero diffractive efficiency. Therefore, the SDO (−1, 3) and (3, −1) are the most difficult SDO to separate and should be given more attention by optical designers.

Secondly, the signs of the 2nd-order and 4th-order aberration coefficients. If the signs of the 2nd-order and 4th-order aberration coefficients are opposite, i.e., $w_{020} w_{040} < 0$, it is possible that the rays from an outer annular of CGH has the zero ray error and cannot be blocked by the pinhole filter. For the SDO with $k_1 + k_2 = 2$, using Eq. (25), the condition to ensure $w_{020} w_{040} > 0$ is

$$(1-\frac{s_0}{r})(1-\frac{r}{s'_0})(1-\frac{s_0}{s'_0})b_m > 0. \tag{27}$$

Thirdly, the ratio $\left|\frac{h_1}{h_3}\right|$. When $\left|\frac{h_1}{h_3}\right| \leq 1$, the CGH in the second pass would be totally covered by the spurious diffraction order and $|\lambda_3| = |h_3| = \lambda_c$ where λ_c is the semi-diameter of the CGH. When $\left|\frac{h_1}{h_3}\right| > 1$, the CGH in the first pass would be total covered and $|\lambda_3| = \left|\frac{h_3}{h_1}\right| \lambda_c < \lambda_c$.

Lastly, the minimum amount of power carrier frequency. Hypothetically, we have the target that the area $\xi > 0.1$ is free of the disturbing of SDO, which means only 1% area of testing part is disturbed. To meet the target, the ray error in Eq. (19) needs to comply with $|e_{ray}| > \frac{D_f}{2}$ at $\xi = 0.1$, where D_f is the aperture of equivalent pinhole filter. Using the 2nd-order aberration in Eq. (25), we calculate that the minimum amount of power carrier frequency for the SDO (−1, 3) and (3, −1) is

$$|s'_0 - s_0| > \sqrt{\frac{5D_f(F\#)}{4\left|(\frac{1}{s'_0}-\frac{1}{r})\right|}} \tag{28}$$

Optics EXPRESS

where $F\#$ is the F number of the aspheric surface ($F\# = \frac{r}{D}$, D is the diameter of the aspheric part).

5. Simulation examples

To validate our aberration model and its qualitative discussion, we calculate the ray error of SDO on equivalent pinhole filter by Eq. (19), calibrate the exit pupil distortion by Eq. (22) and compare our results with those from the real trace when testing different aspheric parts in different CGH layouts. These different aspheric parts and CGH layouts are shown in Table 1 and the figure of the aspheric part is expressed by Eq. (11). All CGHs have the same thickness: 6mm and this thickness is regarded as an equivalent gas layer having the thickness $\frac{6}{n_{cgh}} mm$ in our aberration model where n_{cgh} is the refractive index of CGH. We assume the size D_f of the equivalent pinhole filter is 0.2mm.

Table 1. The basic information of these aspheric parts and CGH layouts

Case number	$F\# = \frac{r}{D}$	$r(mm)$	b_m	PV deviation of aspheric part (um)	s'_0 (mm)	$s_0 - s'_0$ (mm)	CGH semi-diameter. λ_c (mm)
1	1.4	−140	−1	112.7	−52	5.38	21.8
2	1.4	−140	−1	112.7	70	4	21.8
3	2.8	140	−11	75	170	−23.5650	29.8
4	1.4	−140	−1	112.7	70	−4	21.8

5.1 Case 1

The aspheric part in case 1 is a concave one ($r < 0$) with the deformed factor $b_m < 0$ and the CGH is laid outside the focus of the transmission sphere ($s'_0 < 0$), similar to the layout in Fig. 1(a). To ensure the testing data from the outer annular of CGH is not disturbed, we need to comply with Eq. (27). Since $r < s_0 < 0$ and $r < s'_0 < 0$, from Eq. (27), we derive $s_0 - s'_0 > 0$ .On the other sides, to keep the area ($\xi > 0.1$) free of the disturbing of SDO, we need to comply with Eq. (28), which means the minimum defocused distance is $|s_0 - s'_0| = 5.38mm$. Therefore, we have $s_0 - s'_0 = 5.38mm$, shown in Table 1.

The ray error of SDO on equivalent pinhole filter is shown in Fig. 7. We can find the ray error calculated by our aberration model agrees well with the real ray-trace results and the coefficients of the 2nd-order and 4th-order aberration have the same sign. Besides our model shows the significant difference between the SDO (−1, 3) and (3, −1).

Using Eq. (26), we have $\left|\frac{h_1}{h_3}\right| > 1$ at $k_1 > 1$. This is the reason why the SDO (3, −1) only covers half area of CGH ($|\bar{x}_3| < 10mm$) while the SDO (−1, 1), (−1, 3) and (1, −1) can cover the whole CGH in the second pass, as shown in Fig. (7).

The ray error in the inner area of CGH ($|\bar{x}_3| < 0.1\lambda_c$) is clearly shown in Fig. 8. We find that all spurious diffraction orders have the ray error larger than $\frac{D_f}{2} = 0.1mm$ at $|\bar{x}_3| = 0.1\lambda_c$ and can be blocked by the pinhole filter, i.e., we meet the target that the area ($\xi > 0.1$) is free of the disturbing of SDO.

Optics EXPRESS

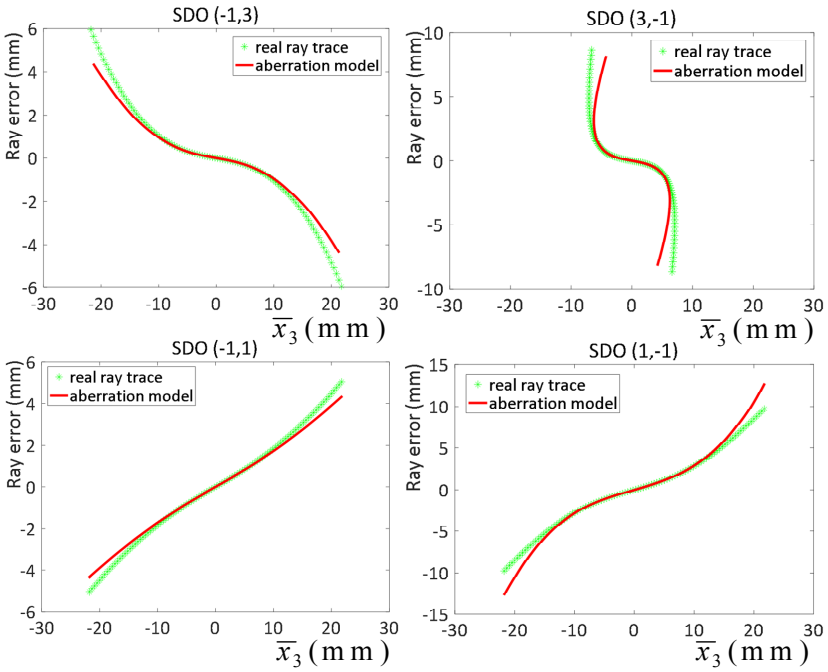

Fig. 7. The ray error vs. $\bar{x}_3$ in case 1. The ray error and $\bar{x}_3$ are the X-axis coordinate of the real ray on equivalent pinhole filter and on the CGH in the second pass, respectively.

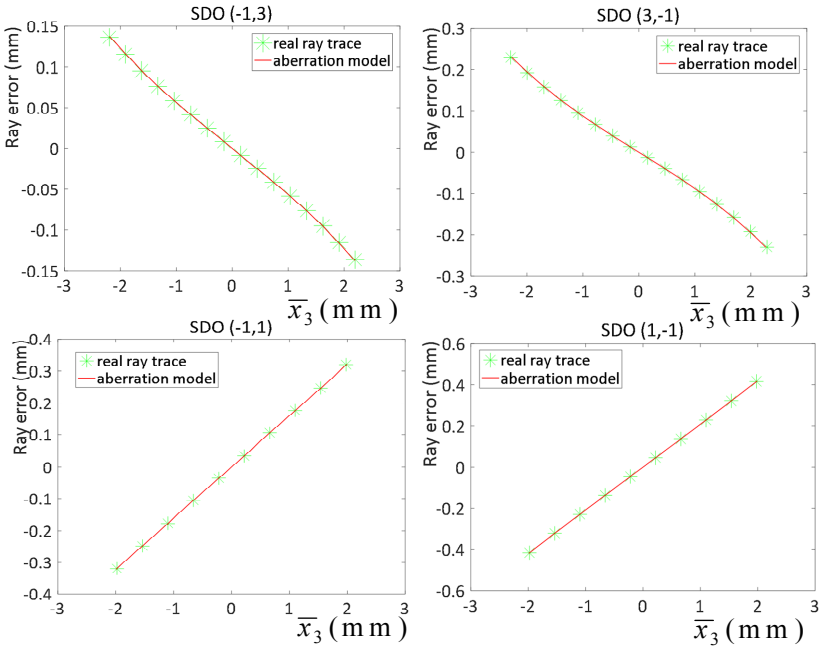

Fig. 8. The ray error vs. $\bar{x}_3$ in case 1 (only plot the area with $|\bar{x}_3| < 2.1mm$).

Optics EXPRESS

5.2 Case 2

The aspheric part in case 2 is the same as that in case 1 but CGH is laid inside the focus of the transmission sphere, as shown in Fig. 1(b). It is easy to find $s_0 > 0, s'_0 > 0$ and $r < 0$ in this case. Similarly to the discussion in case 1, the condition to comply with Eq. (27), 28) is $s_0 - s'_0 > 0$ and $|s_0 - s'_0| = 4mm$, respectively. Therefore, we have $s_0 - s'_0 = 4mm$, shown in Table 1.

From Fig. 9, we find the ray error calculated by our aberration model also agrees well with the real ray-trace results when laying the CGH inside the focus of the transmission sphere. The significant difference between the SDO (k_1, k_2) and (k_2, k_1) is clearly shown. However, instead of $\left|\frac{h_1}{h_3}\right| > 1$ at $k_1 > 1$ in case 1, we have $\left|\frac{h_1}{h_3}\right| > 1$ at $k_1 < 1$ by Eq. (26), so it is the SDO with $k_1 < 1$ that cannot cover the whole CGH in the second pass in Fig. 9.

The pupil distortion of SDO (−1, 3) is shown in Fig. 10. It is easy to see the 3rd-order distortion calculated by our aberration model agrees well with the actual distortion. In addition, there are two different x_3 corresponding to the same $\bar{x}_3$, which means two rays pass through the exit pupil at the same $\bar{x}_3$. This is also the reason why we find two ray errors at one $\bar{x}_3$ in Fig. 9 for SDO (−1, 3).

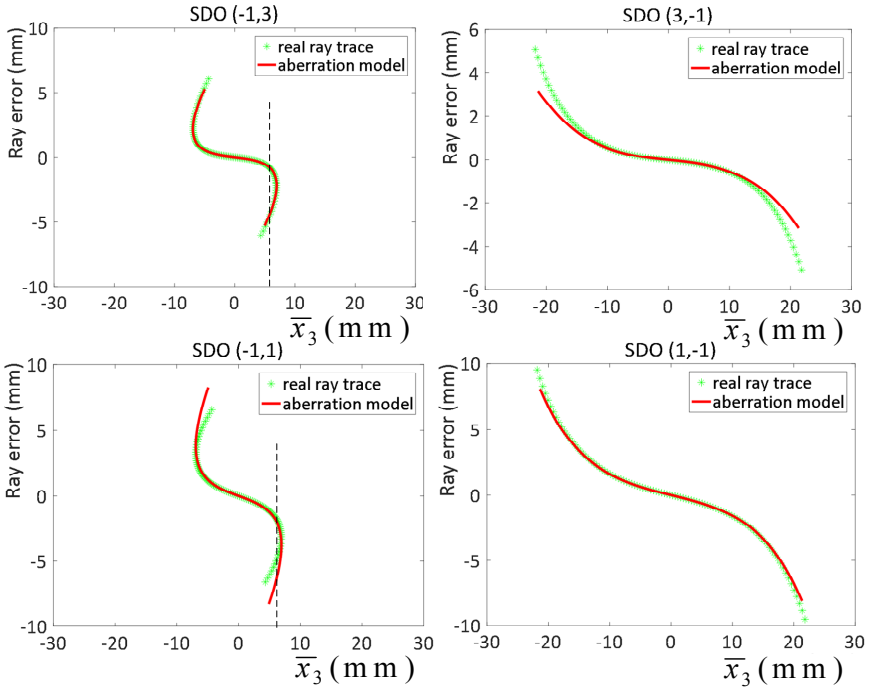

Fig. 9. The ray error vs. $\bar{x}_3$ in case 2. The ray error and $\bar{x}_3$ are the X-axis coordinates of the real ray on equivalent pinhole filter and on the CGH in the second pass, respectively.

Optics EXPRESS

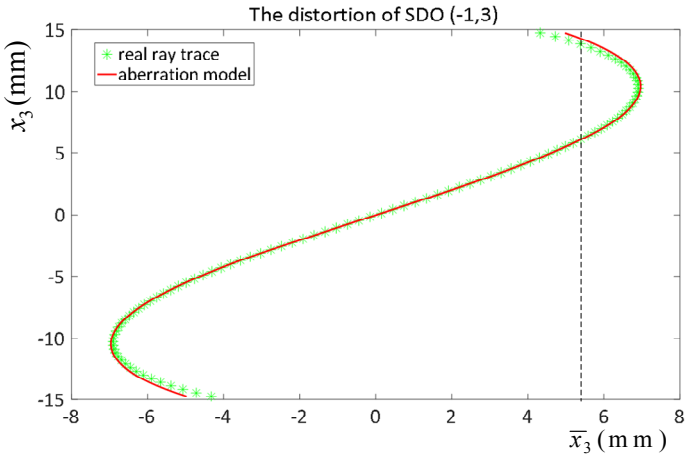

Fig. 10. The pupil distortion of SDO (–1, 3) in case 2. x_3 and $\overline{x}_3$ are the X-axis coordinates of the paraxial and real ray on the CGH in the second pass, respectively. The green marks are the actual distortion calculated by real ray trace and the red line is the 3rd-order distortion calculated by our aberration model with Eq. (22).

5.3 Case 3

The aspheric part in case 3 is a convex one ($r > 0$) with the deformed factor $b_m < 0$, as shown in Fig. 1(c). Because of $0 < r < s_0$ and $0 < r < s'_0$, instead of $s_0 - s'_0 > 0$ in case 1 and 2, we should keep $s_0 - s'_0 < 0$ to comply with Eq. (27) in case 3. By using Eq. (28), we calculate the minimum defocused distance $|s_0 - s'_0|$ is $23.5mm$. Therefore, we have $s_0 - s'_0 = -23.5mm$, shown in Table 1.

The ray error in Fig. 11 demonstrates our aberration model can also be used to analyze the SDO when testing convex aspherical part.

Optics EXPRESS

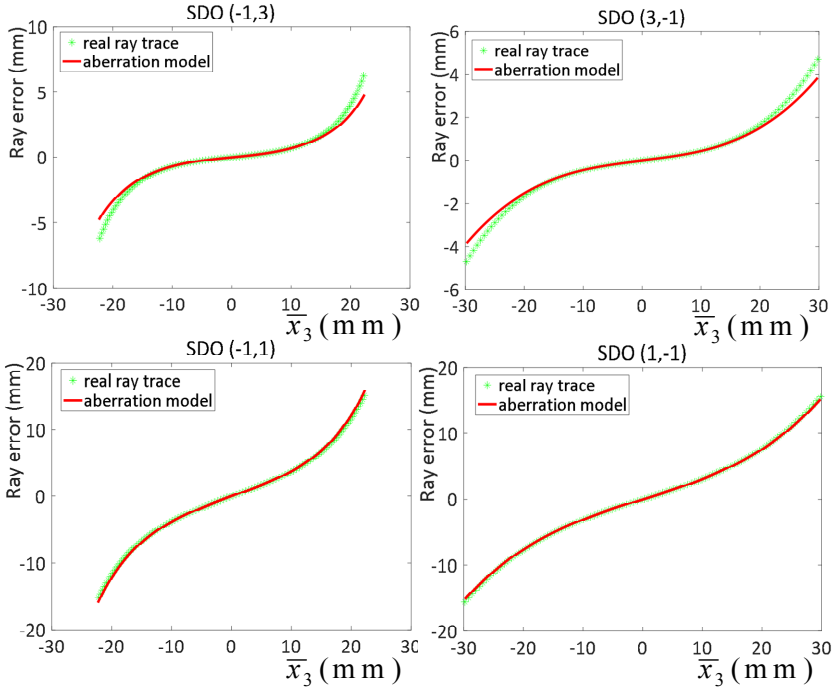

Fig. 11. The ray error vs. $\overline{x}_3$ in case 3. The ray error and $\overline{x}_3$ are the X-axis coordinates of the real ray on equivalent pinhole filter and on the CGH in the second pass, respectively.

5.4 Case 4

Case 4 is the same as case 2, except for the sign of the defocused distance $s_0 - s'_0$, as shown in Table 1. According to the discussion in case 2, if we want the 2nd-order and 4th-order aberrations have the same sign, $s_0 - s'_0$ needs to be larger than zero. In case 4, we intentionally set $s_0 - s'_0 < 0$ and check whether we have a failure in CGH design. According to the ray error of SDO (3, –1) in Fig. 12, we find the ray error is less than 0.1mm ($\frac{D_f}{2}$) in a large area where the testing data also corrupt. Therefore, the case 4 is totally a failure in CGH design.

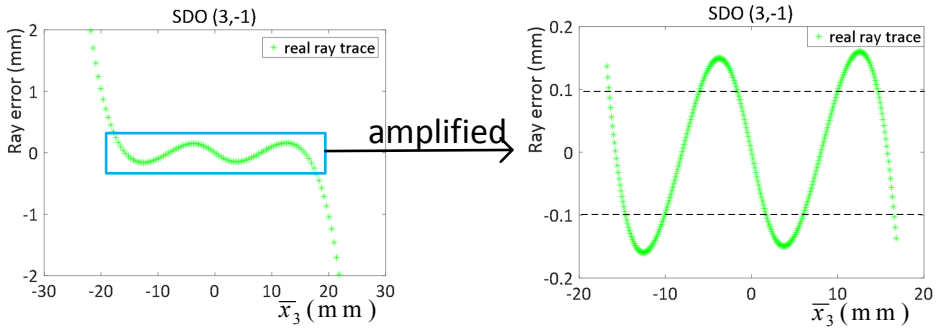

Fig. 12. The ray error vs. $\overline{x}_3$ in case 3. The ray error and $\overline{x}_3$ is the X-axis coordinates of the real ray on equivalent pinhole filter and on the CGH in the second pass, respectively.

Optics EXPRESS

6. Remarks

In this paper, we treat the CGH null system as an imaging system. Based on the Seidel formalism, we build a new aberration model to analyze the effect of spurious diffraction orders of CGH. Compared with the N. Lindlein's model, our model can analyze the difference between the SDO (k_1, k_2) and (k_2, k_1). Since our model considers the effect of the pupil distortion, even if there are two rays passing the same point on the CGH in the second pass, the ray error calculated by our model also agrees well with that calculated by real ray trace.

To carry out the qualitative analysis easily, the 2nd-order and 4th-order aberration coefficients are expanded into a series of $\sum_i \frac{c_i}{a^i}$. From this expansion, we argue that the SDO with $k_1 + k_2 = 2$ has a larger disturbing on testing data than those with $k_1 + k_2 \neq 2$.We derive the condition to ensure that the 2nd-order and 4th-order aberrations have the same sign, which is important to design a successful CGH. We also calculate the minimum defocused distance (power carrier frequency) of CGH, based on the target that the region $\xi > 0.1$ is free of the disturbing of SDO. According to the marginal-ray height (h_1 and h_3) on the CGH in the first and second pass, we provide an equation to determine what kind of SDO will cover the whole CGH in the second pass.

We provide four CGH designs and analyze their SDO. These cases demonstrate that our aberration model is feasible whether the aspheric part is convex or concave and whether the CGH is inside or outside the focus of the transmission sphere.

Funding

China Scholarship Council (501100004543).